Lactate inhibits ATP6V0d2 expression in tumor-associated macrophages to promote HIF-2α–mediated tumor progression

Na Liu,[1] Jing Luo,[1] Dong Kuang,[2,3] Sanpeng Xu,[2,3] Yaqi Duan,[2,3] Yu Xia,[1] Zhengping Wei,[1] Xiuxiu Xie,[1] Bingjiao Yin,[1] Fang Chen,[1] Shunqun Luo,[4] Huicheng Liu,[1] Jing Wang,[1] Kan Jiang,[5] Feili Gong,[1] Zhao-hui Tang,[6] Xiang Cheng,[7] Huabin Li,[8] Zhuoya Li,[1] Arian Laurence,[9] Guoping Wang,[2,3] and Xiang-Ping Yang[1]

[1]Department of Immunology, School of Basic Medicine, Tongji Medical College, Huazhong University of Science and Technology (HUST), Wuhan, China. [2]Institute of Pathology, Tongji Hospital, HUST, Wuhan, China. [3]Department of Pathology, School of Basic Medicine, and [4]The Center for Biomedical Research, Tongji Hospital, Tongji Medical College, HUST, Wuhan, China. [5]Biodata Mining and Discovery Section, National Institute of Arthritis and Musculoskeletal and Skin Diseases, NIH, Bethesda, Maryland, USA. [6]Department of Surgery, Tongji Hospital, HUST, Wuhan, China. [7]Laboratory of Cardiovascular Immunology, Institute of Cardiology, Union Hospital, Tongji Medical College, HUST, Wuhan, China. [8]Department of Otolaryngology, Head and Neck Surgery, Affiliated Eye and ENT Hospital, Fudan University, Shanghai, China. [9]Institute of Cellular Medicine, Newcastle University, Newcastle, United Kingdom.

Macrophages perform key functions in tissue homeostasis that are influenced by the local tissue environment. Within the tumor microenvironment, tumor-associated macrophages can be altered to acquire properties that enhance tumor growth. Here, we found that lactate, a metabolite found in high concentration within the anaerobic tumor environment, activated mTORC1 that subsequently suppressed TFEB-mediated expression of the macrophage-specific vacuolar ATPase subunit ATP6V0d2. *Atp6v0d2*^{–/–} mice were more susceptible to tumor growth, with enhanced HIF-2α–mediated VEGF production in macrophages that display a more protumoral phenotype. We found that ATP6V0d2 targeted HIF-2α but not HIF-1α for lysosome-mediated degradation. Blockade of HIF-2α transcriptional activity reversed the susceptibility of *Atp6v0d2*^{–/–} mice to tumor development. Furthermore, in a cohort of patients with lung adenocarcinoma, expression of ATP6V0d2 and HIF-2α was positively and negatively correlated with survival, respectively, suggesting a critical role of the macrophage lactate/ATP6V0d2/HIF-2α axis in maintaining tumor growth in human patients. Together, our results highlight the ability of tumor cells to modify the function of tumor-infiltrating macrophages to optimize the microenvironment for tumor growth.

Introduction

Macrophages are key regulators of tissue homeostasis and perform tissue-specific functions, which may be influenced by the local tissue environment (1, 2). The tumor microenvironment (TME) is generated by a pathological tissue structure that contains carcinoma cells, mesenchymal cells, and infiltrating immune cells including tumor-associated macrophages (TAMs) (3, 4). All these components interact with each other to maintain or disrupt the viability of the tumor. TAMs can be abundant within tumors and are characterized by the expression of *Arg1* (arginase 1), *Vegf*, and other markers associated with immune cell inhibition or tumor cell growth (5, 6). The TME is able to alter the phenotype of invading macrophages through a complex array of mechanisms that include cytokines and metabolic intermediates (7).

TAMs can drive tumor expansion through the promotion of tumor vascularization via the production of VEGF (8). Key to this is the expression of the 2 transcription factors, HIF-1α and HIF-2α,

within TAMs that mediate VEGF production (9, 10). In an oxygen-rich environment, expression of these 2 proteins is limited by oxygen-dependent proteasome-mediated degradation (11). The TME is typically hypoxic, as the highly metabolically active cells outstrip their blood supply. Even in the presence of an adequate oxygen supply, tumor cells remain highly glycolytic, generating a significant amount of lactate that facilitates tumor growth via HIF-dependent and -independent pathways (12, 13). Both hypoxia and lactate are able to enhance macrophage expression of *Vegf* and *Arg1* (13). Despite much work in the field, the full array of molecular circuits that exist within the TME to prime macrophages into a protumorigenic phenotype remains incomplete.

Cancer cells typically have disordered autophagy that includes disruption of their lysosomal machinery, resulting in the accumulation of damaged organelles and misfolded, potentially toxic proteins (14). The vacuolar ATPases (V-ATPases) are large protein complexes that consist of a peripheral V1 domain that hydrolyzes ATP and an integral V0 domain that transports hydrogen ions, acidifying intracellular compartments including lysosomes, which is required for the completion of autophagy (15). Dysregulation of either the ATPase activity or expression of V-ATPase subunits has been linked with a variety of cancers (16). Within cancer cells, V-ATPases have been reported to play crucial functions in Wnt, Notch, and mTOR signaling that can contribute to cancer cell sur-

vival as well as invasion, migration, and metastasis in the highly acidic TME (17). By contrast, the function of V-ATPases in the accessory cells of the TME has yet to be fully explored.

Here, we found that tumor cell–derived lactate actively downregulates *Atp6v0d2* expression in TAMs via mTOR-dependent inhibition of the transcription factor regulator of lysosomal proteins, TFEB. We found that subcutaneously transplanted tumor cells grew more rapidly in *Atp6v0d2*^{-/-} mice due to enhanced expression of protumoral factors in the TAMs including VEGF production. Expression of these factors is enhanced by HIF-2α. We found that ATP6V0d2 mediates lysosomal degradation of HIF-2α in macrophages, limiting its expression. Inhibition of HIF-2α reversed the phenotype observed in the *Atp6v0d2*^{-/-} mice. Furthermore, ATP6V0d2 expression is positively correlated with survival of a cohort of lung adenocarcinoma patients. Taken together, these results identify what we believe is a novel mechanism by which tumor cells actively downregulate the expression of the macrophage lysosomal gene *Atp6v0d2*, which results in enhanced tumor vascularization and growth via the maintenance of HIF-2α.

Results

Tumor-derived lactate suppresses ATP6V0d2 expression in macrophages. V-ATPases are critical for lysosome acidification and function. To investigate the potential regulation of macrophage lysosome function by tumor cells, we cocultured bone marrow–derived macrophages (BMDMs) with Lewis lung carcinoma–derived (LLC-derived) tumor-conditioned medium (TCM) for 6 hours and measured the expression of all V-ATPase subunits. While LLC-derived TCM enhanced the expression of multiple V-ATPase subunits, the expression of *Atp6v0d2* was significantly reduced in the presence of TCM (Figure 1A and Supplemental Figure 1A; supplemental material available online with this article; https://doi.org/10.1172/JCI123027DS1). We cultured the macrophages with different ratios of LLC-TCM/complete medium and found that at a ratio of 1:3 or above, TCM strongly suppressed the expression of *Atp6v0d2* (Figure 1B), despite the pH and glucose concentrations being comparable to normal complete medium (data not shown). We repeated this experiment with murine melanoma cell line B16-F10–derived TCM and also found inhibition of *Atp6v0d2* expression by B16-F10 TCM, despite the inhibitory effect being irrespective of the ratios of TCM to fresh medium (Supplemental Figure 1, B and C), which might due to the differential presence of some bioactive agents in the two tumor-derived media. Furthermore, we found that exogenously added common cytokines present within tumors such as IL-1β, IL-6, IL-10, and TGF-β had no effect on *Atp6v0d2* expression (Supplemental Figure 1, D–G). In line with this, neutralizing antibodies against IL-1β, IL-6, IL-10, and TGF-β did not reverse the TCM-mediated inhibition of *Atp6v0d2* expression (Supplemental Figure 1H). In addition, boiled TCM derived from LLC cells, as well as from B16-F10 cells, still inhibited the *Atp6v0d2* in macrophages (Figure 1C and Supplemental Figure 1I), suggesting that the active agent in the TCM was heat resistant and likely to be a low molecular weight metabolite.

Lactic acid is a well-known product of tumor cell glycolysis. We found that the lactate concentration was around 34.5 mM in LLC TCM and 45.2 mM in B16-F10 TCM, compared with 1.3 mM in fresh complete medium (Figure 1D and Supplemental Figure

1J). To test the effect of lactate on *Atp6v0d2* expression, we incubated macrophages with media containing varying concentrations of lactate and found that lactate inhibited *Atp6v0d2* expression in a dose-dependent manner over a range of 2 mM to 50 mM (Figure 1E). To confirm that the inhibition of *Atp6v0d2* was due to the presence of lactate in the TCM, we used various concentrations of monocarboxylic acid transport inhibitor 2-cyano-3-(4-hydroxyphenyl)-2-propenoic acid (CHC) in macrophages to block lactate transport. Addition of CHC (5 mM) almost completely reversed the inhibition of *Atp6v0d2* expression by LLC and partially reversed the inhibition by B16-F10 TCM (Figure 1F and Supplemental Figure 1K).

Atp6v0d2 is a target gene of TFEB, a master regulator of lysosomal biogenesis, which can be phosphorylated by mTORC1 and held inactive in the cytoplasm (18, 19). Next we asked whether lactate inhibited *Atp6v0d2* through activation of mTORC1. LLC TCM and boiled LLC TCM, as well as lactate, induced ribosomal protein S6 phosphorylation, a surrogate marker of mTORC1 activation (Figure 1, G and H). This was associated with significantly reduced nuclear localization of TFEB upon lactate or TCM treatment (Figure 1I). Using ChIP combined with quantitative real-time PCR (qPCR), we found that TFEB directly bound to the *Atp6v0d2* promoter and the binding of TFEB was significantly reduced by the addition of lactate or TCM (Figure 1J). Lastly, addition of the mTOR inhibitor Torin reversed the downregulation of *Atp6v0d2* expression by lactate or TCM (Figure 1, K and L).

Atp6v0d2^{-/-} *mice were more susceptible to tumor deposit growth.* To investigate the potential role of macrophage ATP6V0d2 in tumor growth, we injected LLC cells subcutaneously into WT and *Atp6v0d2*^{-/-} mice and monitored the tumor size daily. Deletion of *Atp6v0d2* led to significantly increased tumor size (Figure 2A). The tumor weight was significantly increased in the *Atp6v0d2*^{-/-} mice compared with WT control at day 14 (Figure 2, B and C), suggesting that macrophage ATP6V0d2 suppresses tumor growth. We repeated the experiment with B16-F10 melanoma cells and obtained similar results (Figure 2, D–F).

ATP6V0d2 is expressed in BMDMs and TAMs but not in CD4^{+} or CD8^{+} T cells and tumor cells (Figure 2G, and Supplemental Figure 2, A and B), indicating that the increased tumor growth seen in *Atp6v0d2*^{-/-} mice was due to altered macrophage function. Deletion of *Atp6v0d2* did not alter the number of tumor-infiltrating CD4^{+} and CD8^{+} T cells (Supplemental Figure 2, C–E) or the presence of CD4^{+}FOXP3^{+}, CD4^{+}IFN-γ^{+}, and CD8^{+}IFN-γ^{+} within LLC tumors (Supplemental Figure 2, F–H).

To confirm that the effect of *Atp6v0d2* deletion on tumor cell growth was intrinsic to TAM function, we coinjected LLC cells with either WT BMDMs or *Atp6v0d2*^{-/-} BMDMs into *Atp6v0d2*^{-/-} mice and monitored tumor growth. Compared with the groups with or without WT BMDMs, tumor growth was significantly enhanced in the presence of *Atp6v0d2*^{-/-} BMDMs (Figure 2, H–J). We obtained similar data with coinjection of B16-F10 cells with WT or *Atp6v0d2*^{-/-} BMDMs (Supplemental Figure 3, A–C).

To address this discrepancy, we investigated the functions of ATP6V0d2 in TAMs. WT mice were irradiated and transplanted with BMs either from WT mice or *Atp6v0d2*^{-/-} mice, followed with xenograft of LLC tumor cells. Consistently, mice transplanted
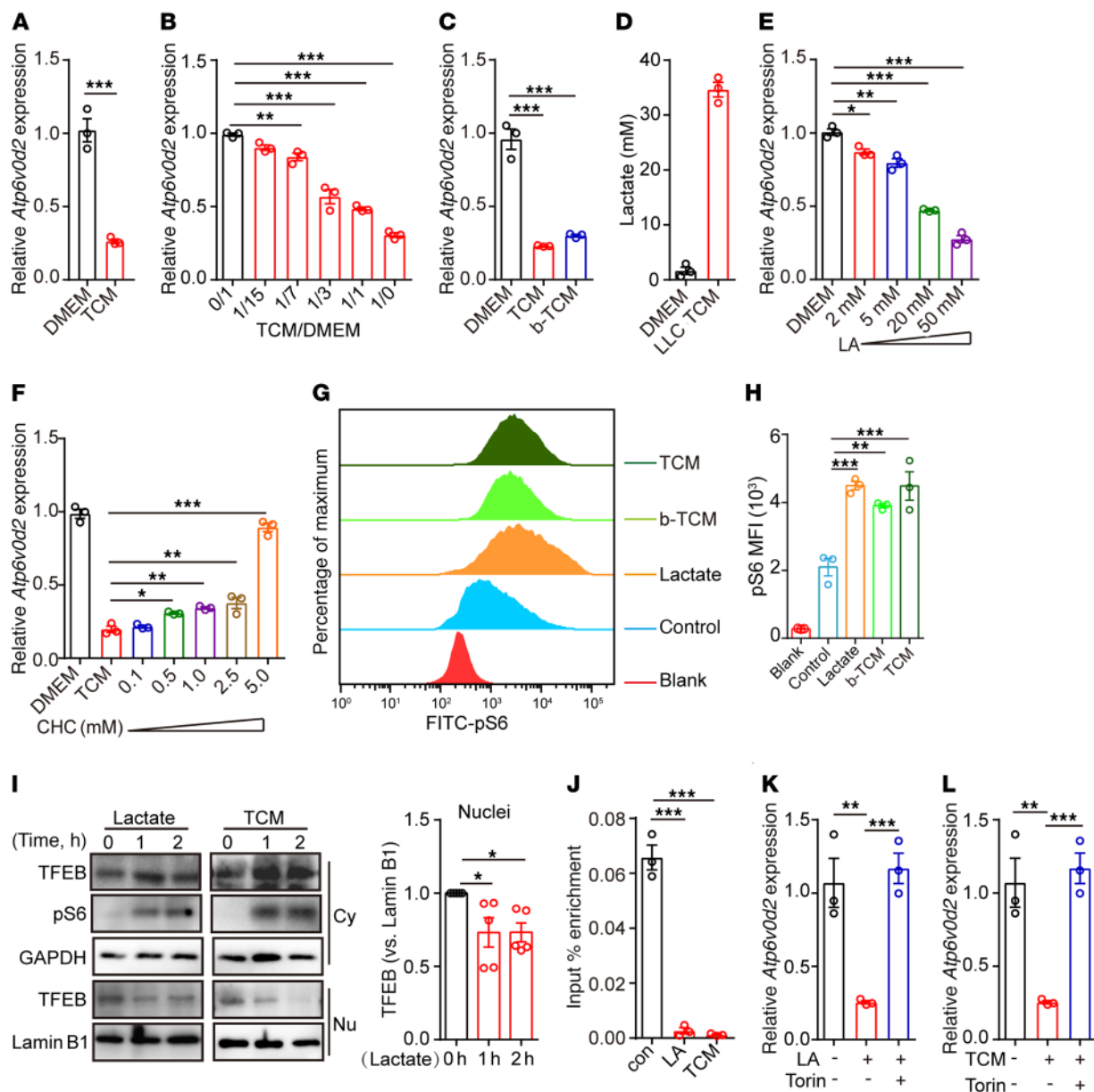
Figure 1. Lactate activates mTORC1 signaling to suppress *Atp6v0d2* expression in macrophages. (**A**–**C**, **E**, and **F**) *Atp6v0d2* mRNA expression was determined by qRT-PCR. (**A** and **B**) LLC tumor-conditioned medium (TCM) was collected after 5 days culture of LLC cells (100% confluence). BMDMs were stimulated with LLC TCM (**A**) or a concentration gradient of LLC TCM (**B**) for 6 hours. (**C**) BMDMs were stimulated with medium, LLC TCM, or boiled LLC TCM (b-TCM; 100°C, 5 minutes) for 6 hours. (**D**) Lactate concentration in LLC TCM was determined. (**E**) BMDMs were stimulated with a concentration gradient of lactate for 6 hours. (**F**) BMDMs were stimulated with LLC TCM alone, or with the addition of different doses of 2-cyano-3-(4-hydroxyphenyl)-2-propenoic acid (CHC), a monocarboxylate channel transporter inhibitor. (**G** and **H**) Representative histograms (**G**) and bar chart (**H**) show the mean fluorescence intensity (MFI) for pS6 expression on macrophages that were starved with Earle's balanced salt solution (EBSS) for 2 hours, followed by replacement with fresh medium (control), or fresh medium with lactate, b-TCM, or TCM for 1 hour. (**I**) BMDMs were starved with EBSS for 2 hours, followed by replacement with fresh medium in the presence of lactate (40 mM) or complete TCM for the indicated times. The amounts of nuclear-cytoplasmic fractionation of TFEB and pS6 were determined by immunoblot and amounts of TFEB in the nuclei were quantified relative to lamin B1. (**J**) RAW264.7 cells were stimulated with lactate (40 mM) or TCM for 4 hours and the binding of TFEB in the *Atp6v0d2* promoter was determined by chromatin immunoprecipitation. (**K** and **L**) BMDMs were stimulated with lactate (**K**) or TCM (**L**) for 6 hours in the presence or absence of 15-minute pretreatment with Torin (1 μM). *Atp6v0d2* mRNA expression was determined by qRT-PCR. Data are representative of 3 independent experiments (**A**–**I**). Data were assessed by unpaired Student's *t* test (**A**), 1-way ANOVA with Turkey's test (**B**, **C**, **E**, **F**, and **L**) and are represented as mean ± SEM. *$P < 0.05$, **$P < 0.01$, ***$P < 0.001$. LA, lactate.

with *Atp6v0d2*-deficient BMs had enhanced tumor growth, and macrophages from that group displayed a more protumoral phenotype (Supplemental Figure 3, D–F), compared with animals transplanted with WT BM.

Together, these data demonstrate that macrophage-expressed ATP6V0d2 inhibits tumor growth in vivo.

Atp6v0d2⁻/⁻ mice were more susceptible to lung metastasis. To investigate whether ATP6V0d2 plays a role in tumor metastasis,
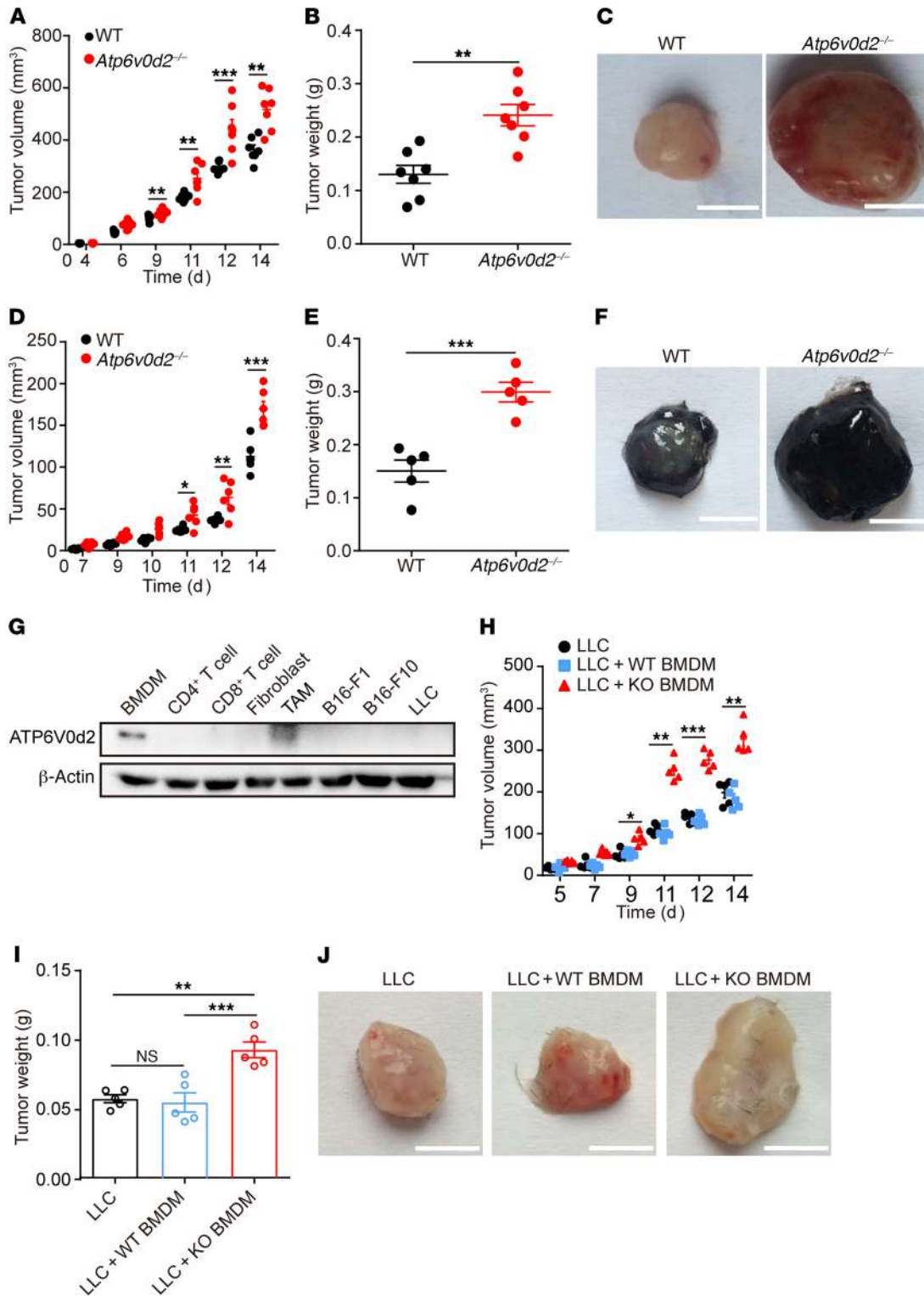
Figure 2. *Atp6v0d2*−/− mice are more susceptible to tumorigenesis. (**A**–**C**) Comparison of LLC tumor growth in WT and *Atp6v0d2*−/− mice (*n* = 7) after implantation: tumor growth rate (**A**), tumor weight (**B**), and representative images of excised tumors (**C**). (**D**–**F**) Tumor growth of B16-F10 in WT and *Atp6v0d2*−/− mice (*n* = 5) after implantation: tumor growth rate (**D**), tumor weight (**E**), and representative images of excised tumors (**F**). (**G**) Immunoblot analysis of ATP6V0d2 expression in macrophages, CD4+ T cells, CD8+ T cells, fibroblasts, TAMs, B16-F1, B16-F10, and LLC cells. (**H**–**K**) *Atp6v0d2*−/− mice were challenged s.c. with 5 × 10⁵ LLC cells alone, or together with 2 × 10⁵ either WT BMDMs or *Atp6v0d2*−/− BMDMs (*n* = 5). Tumor size was measured every 2 to 3 days (**H**). Tumor mass was determined at day 15 after inoculation (**I**). Representative images of tumors are presented (**J**). All experiments except **H**–**J** were repeated 2 times. Data were assessed by unpaired Student's *t* test (**A**, **B**, **D**, and **E**) or 1-way ANOVA with Turkey's post hoc test (**H** and **I**) and are represented as mean ± SEM. *$P < 0.05$; **$P < 0.01$; ***$P < 0.001$. NS, not significant. Scale bars: 5 mm (**C**, **F**, and **J**).
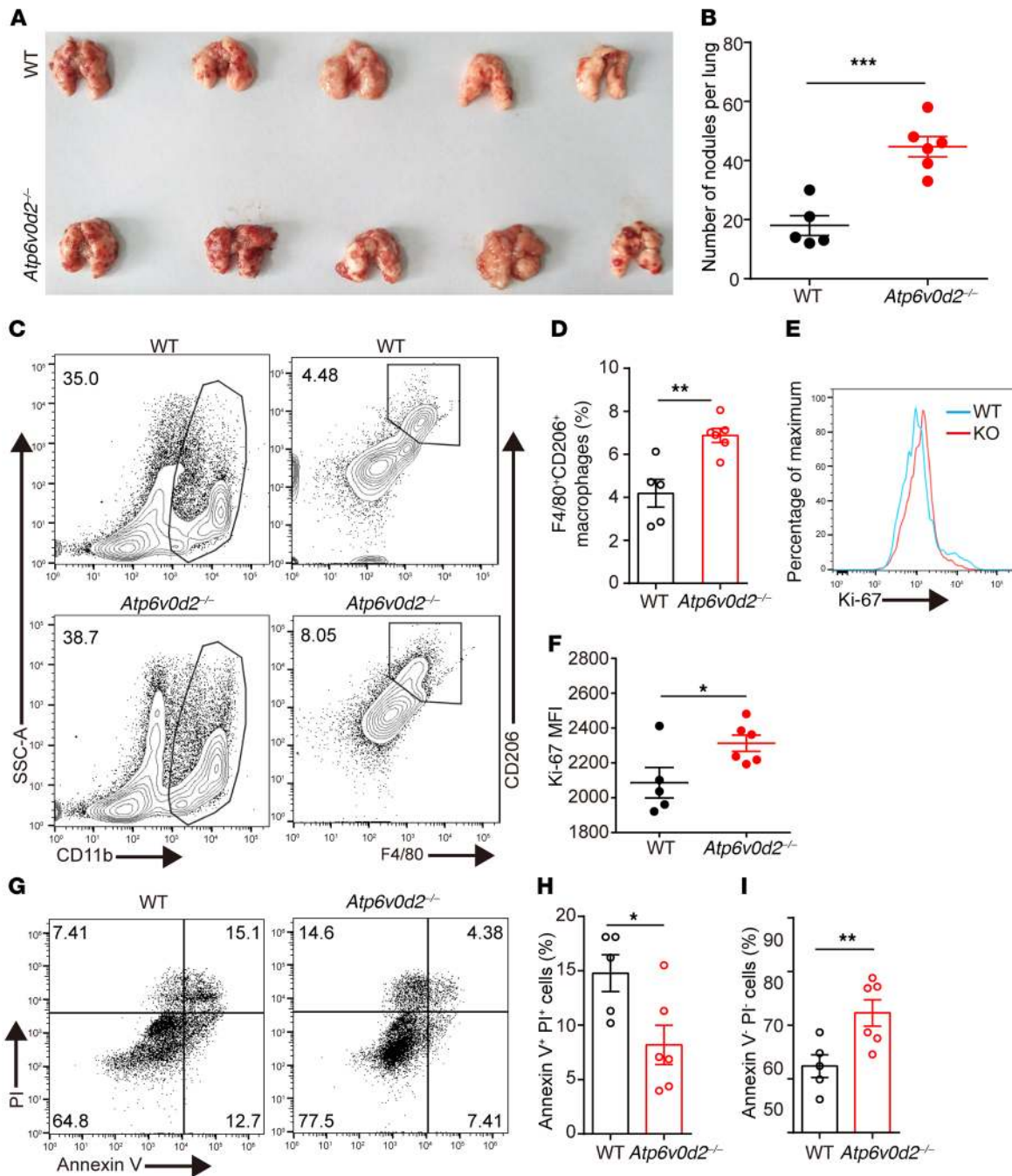
Figure 3. *Atp6v0d2*-deficient mice were more susceptible to lung metastasis. (**A**–**I**) WT and *Atp6v0d2*$^{-/-}$ mice were injected i.v. with 8×10^5 LLC cells. On day 15 after injection, mice were sacrificed. (**A** and **B**) Images (**A**) and quantification analysis (**B**) of lung metastasis of WT (*n* = 5) and *Atp6v0d2*$^{-/-}$ mice (*n* = 6). (**C** and **D**) Flow cytometric analysis of CD11b⁺F4/80⁺CD206⁺ TAMs in lung tissues (**C**) and comparison of fractions of F4/80⁺CD206⁺ TAMs between WT and *Atp6v0d2*$^{-/-}$ mice (**D**). (**E** and **F**) Ki-67 expression by tumor cells in the lung tissues isolated from WT and *Atp6v0d2*$^{-/-}$ mice. (**G**–**I**) Flow cytometric analysis of tumor cell apoptosis in the lung tissues from WT and *Atp6v0d2*$^{-/-}$ mice (**G**), and quantification of apoptotic cells (**H**) and live cells (**I**). Data were assessed by Student's *t* test and are presented as mean ± SEM (*n* = 5–6). *$P < 0.05$, **$P < 0.01$, ***$P < 0.001$.

we inoculated age- and sex-matched WT and *Atp6v0d2*$^{-/-}$ mice with LLC cells intravenously and examined their lungs for metastases. *Atp6v0d2*$^{-/-}$ mice exhibited significantly more tumor nodules (Figure 3, A and B). In the lungs from *Atp6v0d2*$^{-/-}$ mice, the percentages of protumoral CD11b⁺F4/80⁺CD206⁺ cells were significantly higher, compared with those from WT mice (Figure 3, C and D). Furthermore, the metastasized tumor cells (gated on CD45⁻) iso-

lated from the lungs of *Atp6v0d2*$^{-/-}$ mice expressed higher amounts of Ki-67 (Figure 3, E and F). In addition, the tumor cells from the lungs of *Atp6v0d2*$^{-/-}$ mice were less apoptotic (Figure 3, G–I).

Together, these data demonstrate that ATP6V0d2 suppresses tumor metastasis and tumor cell survival in a lung metastasis model.

Deletion of Atp6v0d2 results in enhanced macrophage polarization into a protumoral phenotype in tumors. TAMs display a spe-

cialized protumoral phenotype. To investigate the contribution of ATP6V0d2 in regulation of macrophage polarization, we quantified the proportion of protumoral TAMs within the LLC-induced tumors. Deletion of *Atp6v0d2* resulted in an increased percentage of CD206+CD11C- protumoral cells within the F4/80+ macrophage compartment but had no effect on the percentage of CD206-CD11C+ proinflammatory macrophages (Figure 4, A and B).

The expression of protumoral macrophage–associated factors such as *Mrc1*, *Arg1*, and *Fizz1* within the tumor tissues was significantly higher in *Atp6v0d2*−/− tumor–bearing mice compared with tumors in control animals, but proinflammatory-associated *Il1b* and *Il6* expression was similar (Figure 4C). Next, we compared the expression levels of macrophage-associated genes in the isolated TAMs between WT and *Atp6v0d2*−/− mice. TAMs isolated from *Atp6v0d2*−/− tumor–bearing mice showed elevated expression of protumoral-related genes including *Mrc1*, *Arg1*, and *Fizz1*, and comparable expression of the proinflammatory-related genes *Il1b* and *Il6* (Figure 4D).

To test if ATP6V0d2 is directly involved in macrophage polarization by TCM, we incubated WT or *Atp6v0d2*−/− BMDMs with LLC TCM. After 36 hours, LLC TCM induced significantly higher expression of *Arg1* and *Fizz1* in *Atp6v0d2*−/− BMDMs, compared with WT BMDMs (Figure 4, E and F). By contrast, the absence of ATP6V0d2 resulted in reduced expression of *Il1b* but not *Il6* in macrophages upon treatment with LLC TCM, compared with WT BMDMs (Figure 4, G and H). We repeated the same experiments with B16-F10–derived TCM and found similar results (Supplemental Figure 4, A–D). Taken together, these data suggest that macrophage-intrinsic ATP6V0d2 suppresses expression of protumoral factors by TAMs.

Deletion of Atp6v0d2 results in enhanced VEGF production and abnormal vascularization. We next turned to identifying the cause of accelerated tumor growth in *Atp6v0d2*−/− mice. Fixed tissue sections of tumors were investigated by immunofluorescence. LLC tumors from *Atp6v0d2*−/− mice had increased vascularization and reduced mature vessel generation as measured by CD31 and α-smooth muscle actin (α-SMA) staining, respectively (Figure 5, A–C), together with increased hemorrhagic areas (Figure 5, D and E). These features led us to measure tumor VEGF, which was significantly enhanced within the tumors that grew in the *Atp6v0d2*−/− mice (Figure 5F). The transcripts of *Vegf*, a main driver for angiogenesis, were enhanced in tumors and isolated TAMs in the *Atp6v0d2*−/− mouse group (Figure 5, G and H). In vitro–derived WT or *Atp6v0d2*−/− macrophages expressed little *Vegf*. The addition of LLC and B16-F10 TCM led to enhanced *Vegf* expression after 6 hours that was significantly greater in the *Atp6v0d2*−/− BMDMs, compared with WT controls (Figure 5, I and J). We found similar results in B16-F10–induced tumors that grew in *Atp6v0d2*−/− mice compared with WT controls (Supplemental Figure 5, A–G).

Together, these data demonstrate that tumor-generated lactate inhibits ATP6V0d2 expression and drives VEGF production in TAMs, resulting in enhanced tumor vascularization.

ATP6V0d2 promotes HIF-2α, but not HIF-1α, lysosomal degradation. Next we turned to how ATP6V0d2 would regulate VEGF. HIF-1α and HIF-2α are 2 major transcription factors that induce VEGF during tumor development (10, 20, 21). *Hif1a* and *Hif2a* mRNA expression in the LLC-derived tumors or TAMs was com-

parable between WT control and *Atp6v0d2*−/− mice (Supplemental Figure 6, A–D). Next, we detected HIF-2α protein expression in LLC-induced tumors with immunofluorescence and found that HIF-2α expression was increased in the *Atp6v0d2*-deficient TAMs, suggesting posttranslational regulation of HIF-2α by ATP6V0d2 (Figure 6, A and B). In addition, lactate induced a rapid increase in HIF-2α expression (Supplemental Figure 6E). Next we measured HIF-2α protein levels in a time-course experiment in WT or *Atp6v0d2*−/− macrophages after incubation with TCM. TCM induced HIF-2α accumulation, while it suppressed ATP6V0d2 expression in WT macrophages; the expression levels of HIF-2α were higher after 2-, 4-, and 6-hour TCM stimulation in the absence of ATP6V0d2 (Figure 6C). By contrast, deletion of ATP6V0d2 did not increase HIF-1α protein concentration upon TCM stimulation (Figure 6C). Retroviral forced expression of ATP6V0d2 inhibited the HIF-2α protein expression, as well as p62 and LC3, after LLC TCM stimulation (Figure 6D). Hypoxia stimulation for 4 hours induced significant accumulation of HIF-1α, as well as HIF-2α. However, deletion of ATP6V0d2 resulted in enhanced HIF-2α but not HIF-1α expression, indicating that the specific regulation of HIF-2α by ATP6V0d2 is oxygen independent (Figure 6E).

Deletion of ATP6V0d2 enhanced HIF-2α stability (Supplemental Figure 6, F and G). Next, we treated WT or *Atp6v0d2*−/− BMDMs with proteasome inhibitor MG132 over a time course. We found that treatment of MG132 led to an accumulation of HIF-2α at 2 hours and persisted until 6 hours in the WT cells, indicating a proteasome-mediated degradation of HIF-2α (Figure 6F). However, HIF-2α protein concentration remained significantly higher in *Atp6v0d2*-deficient cells, compared with WT control in the presence of MG132, suggesting a second proteasome-independent regulation of HIF-2α degradation by ATP6V0d2 (Figure 6F). Next, we tested if ATP6V0d2 regulates HIF-2α lysosomal degradation. Macrophages incubated in the presence of bafilomycin A resulted in enhanced HIF-2α in WT cells but not in *Atp6v0d2*−/− cells, and the expression of ATP6V0d2 and p62 was comparable after bafilomycin treatment (Figure 6G), indicating that ATP6V0d2 mediates HIF-2α degradation through its promotion of lysosomal function. Incubation of macrophages with MG132 led to enhanced accumulation of HIF-1α, and it seems there was a synergistic effect on HIF-1α stability by MG132 and the lysosome inhibitor bafilomycin (Supplemental Figure 6H). However, deletion of ATP6V0d2 did not further stabilize HIF-1α (Supplemental Figure 6H).

Next we asked if ATP6V0d2 affected the localization of HIF-2α within lysosomes. Treatment of macrophages with MG132 to block the proteasome degradation pathway resulted in enhanced colocalization of HIF-2α and LysoTracker in WT cells, whereas the colocalization of HIF-2α and LysoTracker was significantly reduced in the *Atp6v0d2*−/− cells (Figure 6, H and I).

Taken together, these data suggest that ATP6V0d2 promotes lysosomal HIF-2α degradation, but does not alter HIF-1α.

Blockade of HIF-2α activity reversed the enhanced tumorigenesis in Atp6v0d2−/− *mice.* To test the significance of HIF-2α in mediating the effects seen in *Atp6v0d2*−/− macrophages, WT and *Atp6v0d2*−/− mice were injected with LLC tumor cells. At day 10, when the injected LLC tumor cells grew to a size of 100–200 mm³, mice were treated with the HIF-2α inhibitor PT2385 (5 mg/kg) or PBS control twice daily. At day 14, the mice were sac-
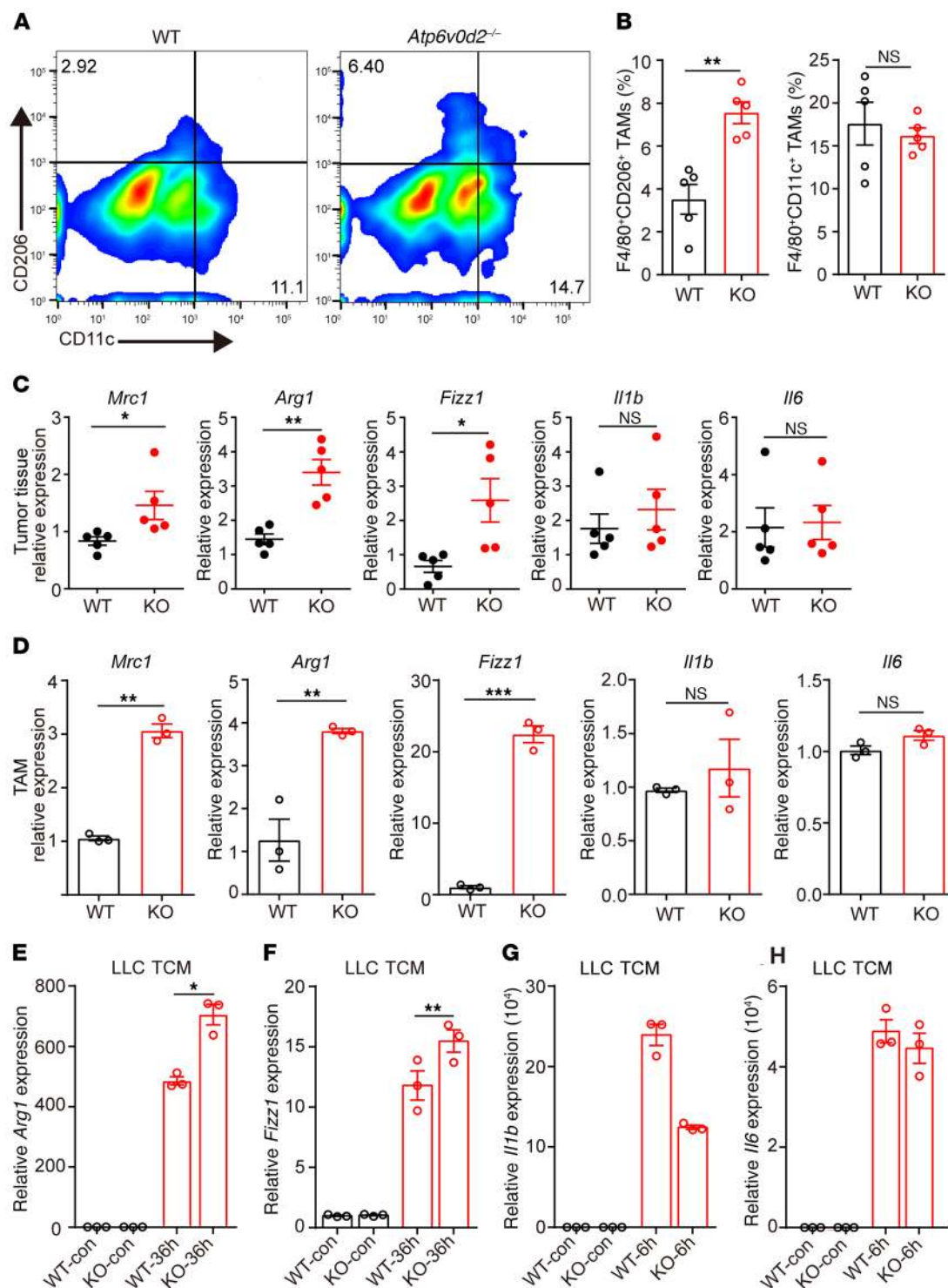
Figure 4. Deletion of *Atp6v0d2* leads to enhanced protumoral polarization of macrophages. (**A–D**) WT and *Atp6v0d2*⁻/⁻ mice were injected s.c. with 5 × 10⁵ LLC cells. On day 15 after inoculation, mice were sacrificed. (**A** and **B**) Representative flow cytometric plots of tumor-infiltrating, gated F4/80⁺cells showing CD11C⁺CD206⁻ (proinflammatory) and CD11C⁻CD206⁺ (protumoral) TAM fractions in LLC tumor xenograft model (**A**) and comparisons of fractions of CD11C⁺CD206⁻ and CD11C⁻CD206⁺ in TAMs between WT and *Atp6v0d2*⁻/⁻ mice (**B**) (*n* = 5). (**C**) The expression of *Mrc1, Arg1, Fizz1, Il1b,* and *Il6* in WT and *Atp6v0d2*⁻/⁻ (KO) tumor tissues was determined by qRT-PCR (*n* = 5). (**D**) TAMs from tumor-bearing WT and *Atp6v0d2*⁻/⁻ mice were isolated with CD11b magnetic beads. The expression of *Mrc1, Arg1, Fizz1, Il1b,* and *Il6* was determined by qRT-PCR (*n* = 5). (**E** and **F**) WT and *Atp6v0d2*⁻/⁻ BMDMs were stimulated with medium or LLC TCM for 36 hours. The expression of *Arg1* (**E**) and *Fizz1* (**F**) was determined by qRT-PCR. (**G** and **H**) WT and *Atp6v0d2*⁻/⁻ BMDMs were stimulated with medium or LLC TCM for 6 hours. The expression of *Il1b* (**G**) and *Il6* (**H**) was determined by qRT-PCR. Data are representative of 2 (**A–D**) or 3 (**E–H**) independent experiments. Data were assessed by unpaired Student's *t* test and are represented as mean ± SEM, *P < 0.05, **P < 0.01, ***P < 0.001. NS, not significant.

rificed. The addition of PT2385 reversed the difference in tumor growth seen between WT and *Atp6v0d2*^{-/-} mice (Figure 7, A and B). At day 14, we found a significant increase in serum VEGF concentration in the *Atp6v0d2*^{-/-} mice that was reversed in animals that received 4 days of PT2385 (Figure 7C). We detected enhanced abnormal vascularization in the tumors of *Atp6v0d2*^{-/-} mice by immunoflorescent staining with anti-CD31 and anti–α-SMA that was reversed by the addition of PT2385 (Figure 7, D–F). Furthermore, the enhanced expression of HIF-2α target genes including *Vegf1*, *Glut1*, *Ccnd1*, and *Pai1* in tumors isolated from *Atp6v0d2*^{-/-} mice was reversed by PT2385 (Supplemental Figure 7, A–D). We obtained similar results for HIF-2α target genes in TCM-stimulated WT and *Atp6v0d2*^{-/-} macrophages (Supplemental Figure 7, E–H). We next measured expression of macrophage genes associated with a protumoral phenotype, including *Mrc1*, *Arg1*, *Fizz1*, and *Ym1* and found their expression enhanced in the tumors isolated from *Atp6v0d2*-deficient mice compared with WT controls; inhibition of HIF-2α transcriptional activity by PT2385 inhibited expression of these genes, eliminating the differences between WT and *Atp6v0d2*-deficient mice (Figure 7, G–J). To confirm that these differences could be explained by differences in expression within macrophages, we incubated WT or *Atp6v0d2*^{-/-} BMDMs in TCM with or without PT2385 and measured protumoral-related gene expression. We saw little gene expression in unstimulated cells. By contrast, TCM induced expression of *Arg1*, *Fizz1*, and *Ym1* in WT BMDMs that was significantly enhanced in *Atp6v0d2*^{-/-} BMDMs (Figure 7, K–M). Lastly, the addition of PT2385 resulted in a significant reduction in the expression of *Arg1*, *Fizz1*, and *Ym1* in both WT and *Atp6v0d2*^{-/-} BMDMs and eliminated the differences between the 2 groups (Figure 7, K–M). Taken together, these data demonstrate that the enhanced HIF-2α contributed to the enhanced vascularization, protumoral macrophage polarization, and tumorigenesis seen in the absence of ATP6V0d2.

Macrophage ATP6V0d2 expression is inversely correlated with both the presence of CD163⁺ *TAMs and survival in human lung adenocarcinoma patients.* To investigate the significance of the ATP6V0d2-mediated HIF-2α lysosomal degradation in human cancers, we measured the expression of ATP6V0d2 and HIF-2α in lung adenocarcinoma tissues (*n* = 35) in patients that have received surgical resection of their lung tumors. While few CD68⁺ macrophages were present in normal lung tissue adjacent to the tumors, there was a significant number of macrophages within tumor tissues (Supplemental Figure 8A); both ATP6V0d2 and HIF-2α expression was restricted to the CD68⁺ macrophages, but not in other leucocytes within lung adenocarcinoma tissue (Supplemental Figure 8B and Figure 8A), despite that HIF-2α was reported in a very small population of non–small cell lung carcinoma samples (22). In contrast, HIF-1α was expressed in tumor cells, as well as infiltrated immune cells (Supplemental Figure 8C), indicating that the undetected HIF-2α in our hands is not due to sample preparation. We divided the lung adenocarcinoma patients into 2 groups on the basis of macrophage ATP6V0d2 expression and found that there were more CD163⁺ protumoral-like macrophages and enhanced HIF-2α in the low-ATP6V0d2-expression group (Figure 8B). Next, we turned to patient survival using Kaplan-Meir survival analysis in patients after undergoing surgical resection of their lung

tumors. We found that the survival time for patients with high ATP6V0d2 expression was significantly extended compared with patients that had low ATP6V0d2 expression (Figure 8C). The proportion of patients expressing ATP6V0d2 in the survival group was higher than that in the deceased group (83% versus 45%) (Figure 8D). Although there was no difference in numbers of CD68⁺ cells within tumors between high-ATP6V0d2-expression and low-ATP6V0d2-expression patients, the numbers of CD163⁺ protumoral-like macrophages were significantly higher in the low-ATP6V0d2-expression group (Figure 8E and Supplemental Figure 8D). Consistent with this, when the patients were divided into 2 groups on the basis of HIF-2α expression, the patients with higher expression levels of HIF-2α had a significantly shorter survival time (Figure 8F). Taken together, these data demonstrate that the ATP6V0d2-mediated HIF-2α lysosomal degradation in macrophages is linked with the survival of human lung adenocarcinoma patients.

Discussion

The reciprocal regulation between tumor cells and tumor-infiltrating immune cells shapes the immune status of the TME and may determine the outcome of cancer progression. Here, we demonstrate that tumor cell–derived lactate suppressed macrophage ATP6V0d2 expression via activation of mTORC1 that led to reduced lysosomal degradation of HIF-2α. Subsequently, macrophages produced more VEGF and were polarized into a protumoral phenotype by lactate. We found that tumors grew faster in *Atp6v0d2*-deficient mice compared with control animals. In tumor deposits from patients, the expression of ATP6V0d2 inversely correlated with HIF-2α expression in TAMs and postoperative survival of lung cancer patients.

Macrophages are influenced by the local environment as sentinels of the immune system and acquire additional activities tailored for their tissue-specific functions (23). mTOR signaling senses and integrates nutrition, growth factors, and energy status to coordinate cellular function. Lactate has been shown to activate PI3K/Akt in endothelial cells through an unknown mechanism and mTOR in tumor cells via glutamine metabolism (24, 25). It is unclear if lactate also activates mTOR via glutamine metabolism in macrophages. V-ATPase is critical for lysosomal acidification. In addition, some subunits have been linked with autophagosomal-lysosomal fusion (26) and have been shown to be regulated by TFEB, the master regulator of lysosomal biogenesis (19). We found that TFEB bound to and regulated the expression of *Atp6v0d2*, and the activation of TFEB was inhibited by lactate in an mTORC1-dependent manner, demonstrating the importance of the TME in macrophage signaling and function.

In contrast with ubiquitous expression of HIF-1α, HIF-2α expression is restricted and plays a significant role in regulating macrophage function in inflammation and cancer (27, 28). Although HIF-1α is required for *Vegf* induction in macrophages, our data demonstrated that dysregulated HIF-2α expression enhanced *Vegf* expression and facilitated tumor growth in both mouse and human, indicating that both HIF members contribute to shaping the macrophages within the TME for them to acquire maximal protumoral activities. Despite the enhanced HIF-2α expression in steady-state *Atp6v0d2*^{-/-} macrophages (Figure 6C),
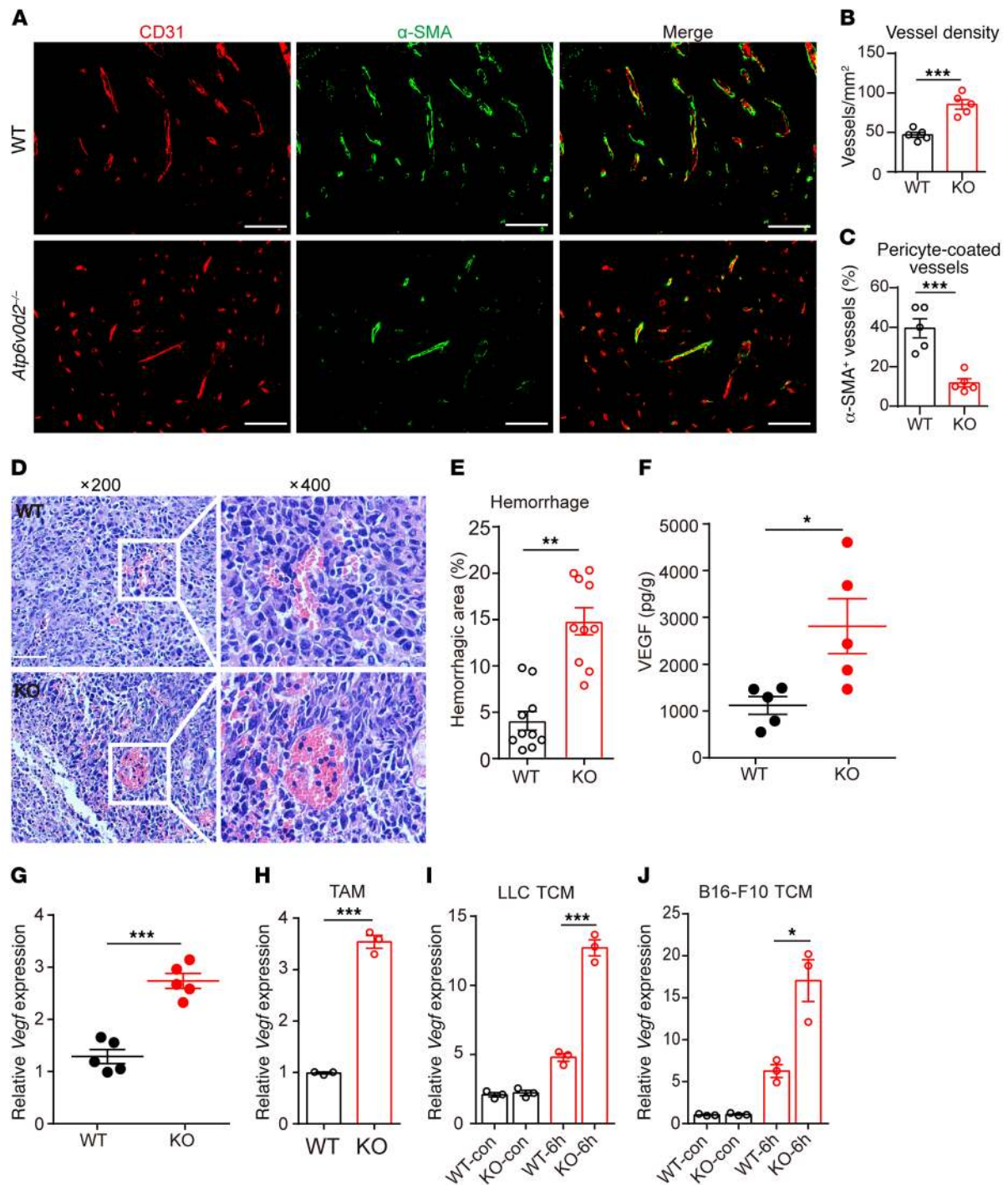
Figure 5. *Atp6v0d2* deficiency results in enhanced tumor angiogenesis. (A–I) WT and *Atp6v0d2*⁻/⁻ mice were injected s.c. with 5 × 10⁵ LLC cells. On day 15 after inoculation, mice were sacrificed (*n* = 5). (**A–C**) Double immunostaining for CD31 (red) and α-SMA (green) vessels in tumor tissues from WT and *Atp6v0d2*⁻/⁻ mice (**A**). Quantification of the percentage CD31⁺ vessels (**B**) and α-SMA⁺CD31⁺ vessels (**C**). (**D** and **E**) H&E staining on tumor tissues in WT and *Atp6v0d2*⁻/⁻ mice. Histogram depicts the percentage of hemorrhagic area versus the whole tumor area (**E**). (**F**) Comparison of tumor tissue VEGF levels at day 15 in WT and *Atp6v0d2*⁻/⁻ mice. (**G** and **H**) The expression of *Vegf* in tumor tissues (**G**) or isolated TAMs (**H**) from WT and *Atp6v0d2*⁻/⁻ mice was determined by qRT-PCR. (**I** and **J**) Expression analysis of *Vegf* by qRT-PCR in WT and *Atp6v0d2*⁻/⁻ BMDMs that were stimulated with LLC TCM (**I**) or B16-F10 TCM (**J**) for 6 hours. Data are representative of 3 independent experiments. Data were assessed by Student's *t* test and are represented as mean ± SEM. *$P <$ 0.05; **$P <$ 0.01; ***$P <$ 0.001. Scale bars: 100 μm.
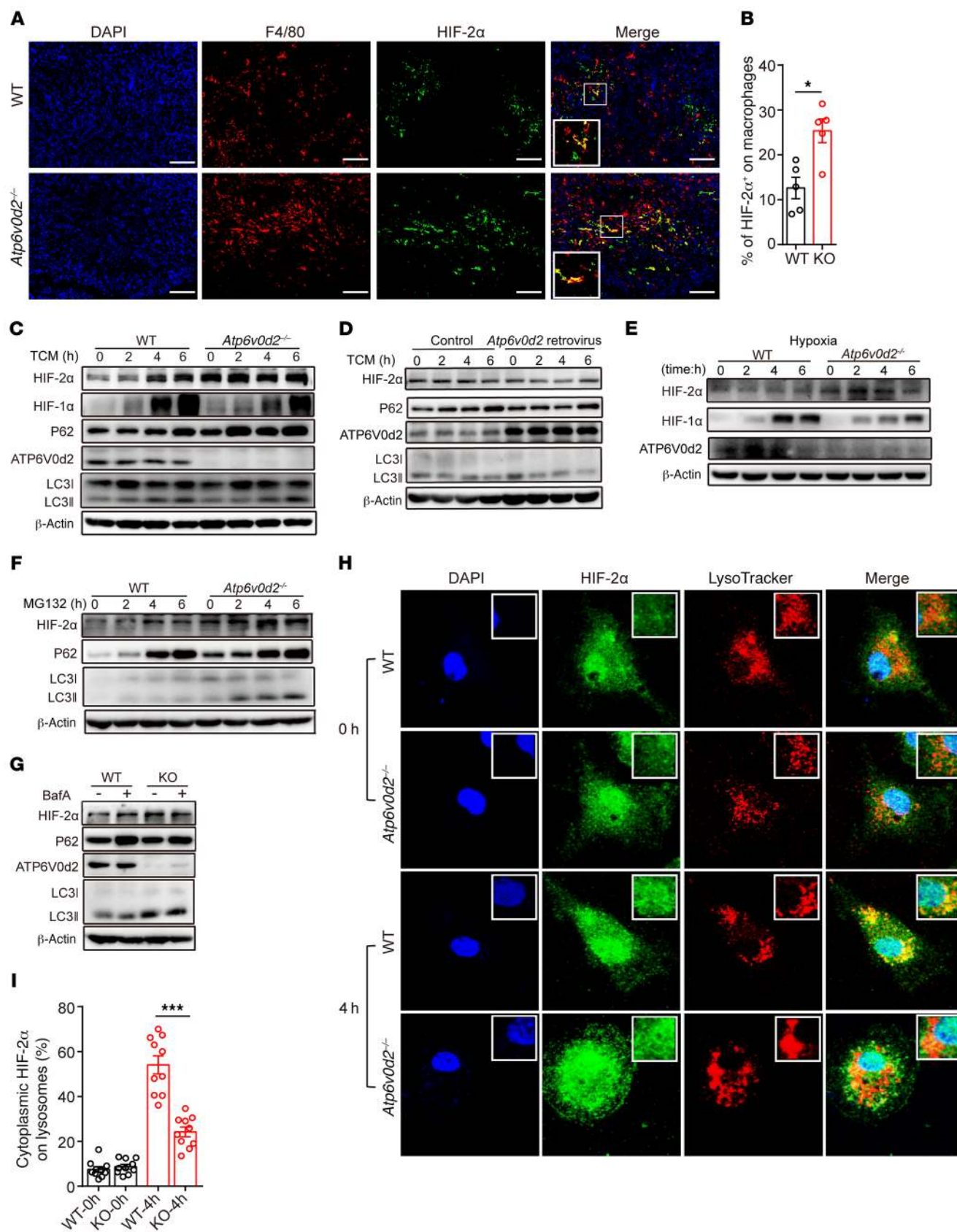
Figure 6. Deletion of *Atp6v0d2* results in enhanced stabilization of HIF-2α. (**A** and **B**) Whole-mount immunofluorescence staining of DAPI (blue), F4/80 (red), and HIF-2α (green) in tumor tissues of WT and *Atp6v0d2⁻/⁻* mice (**A**). Scale bars: 100 μm (original magnification, ×200). Higher-magnification insets are ×400. The percentage of HIF-2α⁺F4/80⁺ among F4/80⁺ cells was quantified manually (**B**). (**C**) Immunoblotting of HIF-2α, HIF-1α, P62, ATP6V0d2, and LC3 in WT and *Atp6v0d2⁻/⁻* BMDMs that were stimulated with LLC TCM for the indicated times. (**D**) WT BMDMs were transduced with control virus or retroviral ATP6V0d2 virus, followed by treatment with LLC TCM for the indicated times. The expression of HIF-2α, P62, ATP6V0d2, and LC3 was determined by immunoblotting. (**E**) Immunoblotting of HIF-2α, HIF-1α, and ATP6V0d2 in WT and *Atp6v0d2⁻/⁻* BMDMs that were stimulated with hypoxia (1% O₂) for the indicated times. (**F**) Immunoblotting of HIF-2α, P62, and LC3 in WT and *Atp6v0d2⁻/⁻* BMDMs that were incubated with MG132 (20 μM) for the indicated times. (**G**) WT and *Atp6v0d2⁻/⁻* BMDMs were untreated, or treated with bafilomycin A (100 nM) for 6 hours. The expression of HIF-2α, P62, ATP6V0d2, and LC3 was determined by immunoblotting. (**H** and **I**) WT and *Atp6v0d2⁻/⁻* BMDMs were untreated or treated with MG132 (20 μM) for 4 hours. Cells were stained with anti–HIF-2α and LysoTracker (**H**). Original magnification, ×630 and ×2,520 (insets). Colocalization of HIF-2α and lysosomes among cytoplasmic HIF-2α was quantified (**I**). Data were assessed by Student's *t* test and are representative of 2 (**A** and **B**) or 3 (**C**–**I**) independent experiments and are presented as mean ± SEM. *P < 0.05, ***P < 0.001.

the VEGF production was similar to that in steady-state WT cells (Figure 5, I and J), indicating that HIF-2α–mediated VEGF production may require other factors, which are activated during TCM stimulation or tumor progression in vivo. Our data, together with a previous report (13), suggest that lactate engages 2 parallel pathways to regulate ATP6V0d2-independent HIF-1α and ATP6V0d2-dependent HIF-2α expression to enhance protumoral activity of macrophages. In contrast to hypoxia-dependent enhancement of HIF-1α protein expression by lactate (data not shown), lactate enhances HIF-2α independently of oxygen level.

The stability of both HIF-1α and HIF-2α expression is classically regulated by the proteasome (29, 30). However, recent studies have demonstrated that these 2 molecules are also subject to lysosome-mediated degradation in cancer cells (31–33). Our work suggests that distinct lysosomal regulation of these 2 related transcription factors exists. Considering the restricted expression of ATP6V0d2, it is highly likely that distinct types of cells may employ different machineries for lysosomal degradation of HIF-2α. Rapamycin promoted HIF-2α degradation in WT macrophages but not in *Atp6v0d2⁻/⁻* macrophages (data not shown), suggesting that ATP6V0d2 promotes HIF-2α degradation via an autophagic process that is dependent on lysosomal degradation. Currently, it remains unclear how ATP6V0d2 selectively regulates HIF-2α stability.

Despite a report that HIF-2α is expressed in a small proportion of human lung adenocarcinomas (34), we found that both ATP6V0d2 and HIF-2α were exclusively expressed in macrophages and that their expression is inversely correlated with each other, consistent with our mouse data. In contrast, HIF-1α is expressed in both tumor cells and tumor-infiltrating immune cells, which is consistent with the idea of differential expression between HIF-1α and HIF-2α (22). The expression level of ATP6V0d2 and HIF-2α in TAMs correlated positively and negatively with patient survival, respectively, highlighting the significance of the regulation of HIF-2α by ATP6V0d2 in human cancers. This could

not be explained by differences in the intratumoral inflammatory infiltrate, as we found similar numbers of TAMs inside human lung cancers with different outcomes. This suggests that the function rather than the number of TAMs is critical for prognosis, consistent with previous studies (35, 36).

In summary, our findings identified ATP6V0d2 as a key factor that mediates the ability of a lactate-enriched TME to induce protumoral activities in TAM via the maintenance of hypoxia-independent regulation of HIF-2α. This scenario provides molecular and cellular insights into the macrophage acquisition of protumoral activities within tumors and expands the number of factors that mediate the effect of the TME.

Methods

Mice. Atp6v0d2⁻/⁻ mice were generated using TALEN (transcription activator–like effector nuclease) technology. A TALEN binding pair was chosen from *Atp6v0d2* CDS in the first exon. The genomic recognition sequences of TALEN left and right arms are CGAGGATG-CAAAGCCAGCC (L) and GCACTAGGTTGACATA (R), spaced by 16 bp and anchored by a preceding T base at the –1 position to meet the optimal criteria for natural TAL proteins. TALEN vectors of left and right arms, TALEN-*Atp6v0d2*-L and TALEN-*Atp6v0d2*-R, were obtained by 1-step ligation using the FastTALE TALEN Assembly Kit (SIDANSAI Biotechnology) according to the manufacturer's instructions. mRNA (400 ng/μl, 10 pl) was injected into the cytoplasm of 180 one-cell embryos. After incubation for 24 hours, the selected 2-cell embryos were transferred into the oviduct of 7 pseudopregnant C57BL/6 mice. We confirmed the genotype of F0 mice by DNA sequencing. C57BL/6 WT mice were purchased from Huafukang. All the mice were bred and housed in a specific-pathogen-free facility at the Tongji Medical College, HUST.

Xenograft mouse tumor models. Male C57BL/6 WT or *Atp6v0d2⁻/⁻* mice were injected s.c. with either 5 × 10⁵ LLC cells or 2 × 10⁵ B16-F10 cells. Tumor growth was measured every 2 to 3 days after tumor inoculation using digital calipers. Mice were sacrificed 14 days after inoculation and tumors were excised and weighed. For macrophage adoptive transfer experiments, *Atp6v0d2⁻/⁻* mice were injected s.c. with 5 × 10⁵ LLC cells alone or 5 × 10⁵ LLC cells plus either 2 × 10⁵ WT BMDMs or *Atp6v0d2⁻/⁻* BMDMs, or injected s.c. with 5 × 10⁵ B16-F10 cells alone or 5 × 10⁵ B16-F10 cells plus either 2 × 10⁵ WT BMDMs or *Atp6v0d2⁻/⁻* BMDMs. Tumor growth and weight were determined as described above.

Generation of BM–chimeric mice. BM chimeras were generated as follows. Briefly, 8- to 12-week-old CD45.2 WT C57BL/6 male mice were sublethally irradiated with 7 Gy of whole-body irradiation. BMs were harvested from donor CD45.2 WT and *Atp6v0d2⁻/⁻* mice or CD45.1 WT mice to monitor the chimeric efficiency. Two hours after irradiation, mice were injected i.v. with 8 × 10⁶ cells from donor BM. After 4 weeks of transplantation, mice were s.c. challenged with 5 × 10⁵ LLC cells. Percentage of chimerism was determined by staining peripheral blood cells with anti-CD45.1-PE (clone A20; BD Biosciences) and anti-CD45.2-APC (clone 104; Biolegend) antibodies for analysis by flow cytometry.

For the inhibition of HIF-2α in a mouse model, a total of 5 × 10⁵ LLC cells in a volume of 100 μl of PBS were inoculated s.c. into 6- to 7-week-old C57BL/6 WT or *Atp6v0d2⁻/⁻* male mice. PT2385 was formulated with 10% absolute ethanol, 30% PEG400, 60% water con-
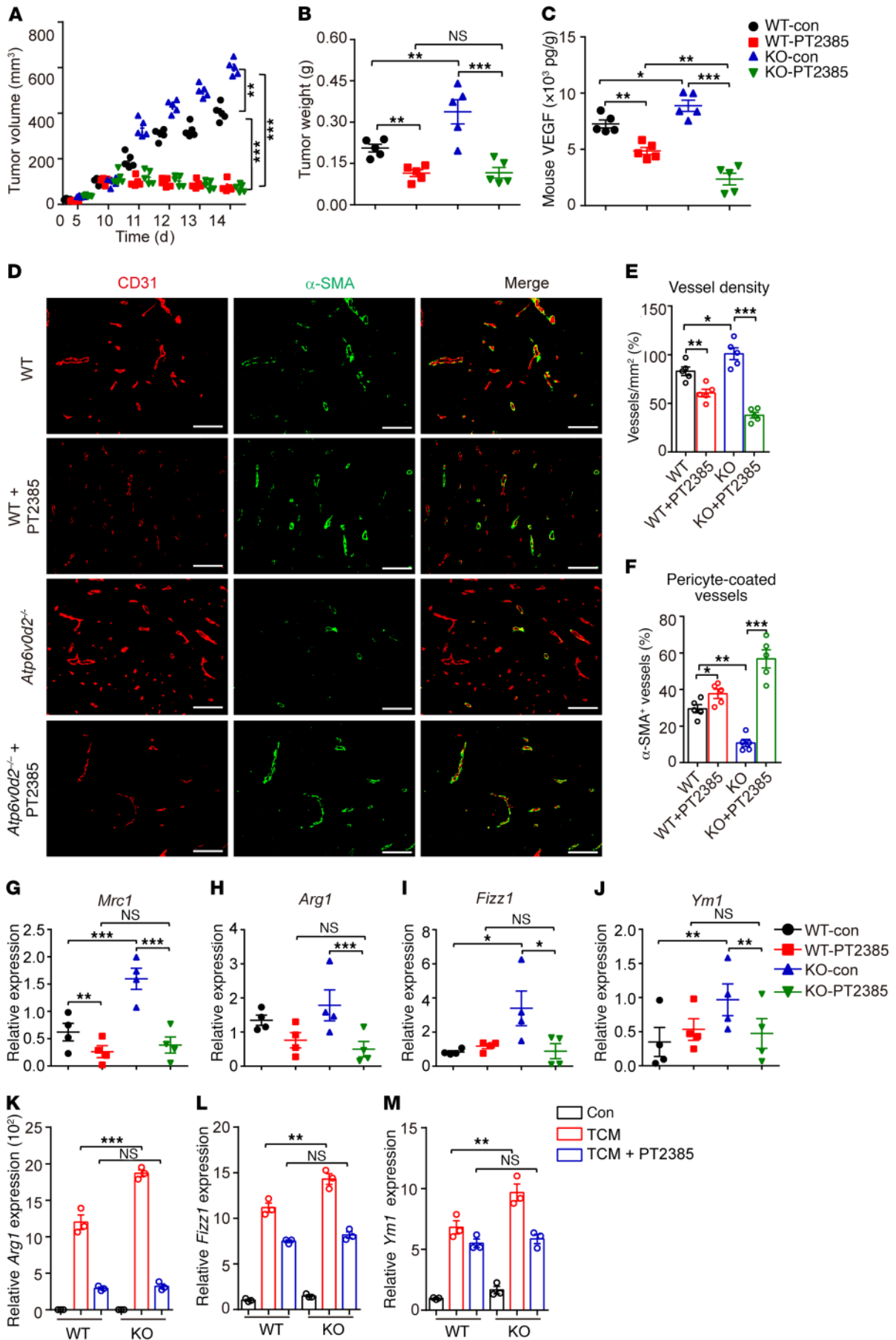
Figure 7. Suppression of HIF-2α activity reverses the enhanced tumorigenesis in *Atp6v0d2*^{-/-} mice. (**A**–**J**) WT and *Atp6v0d2*^{-/-} mice (*n* = 5) were injected s.c. with 5 × 10⁵ LLC cells. Once the tumor volumes reached 100–200 mm³ at around day 10, mice were gavaged with vehicle or HIF-2α inhibitor PT2385 (5 mg/kg) twice daily for 4 consecutive days. Growth curve (**A**) and tumor weight (**B**) were plotted. (**C**) Comparison of tumor tissue VEGF levels. (**D**–**F**) Immunostaining of CD31 and α-SMA in tumor tissues (**D**) and quantification of CD31⁺ area percentage (**E**), CD31⁺α-SMA⁺ vessels as a percentage of CD31⁺ vessels (**F**) in the tumor areas. (**G**–**J**) qRT-PCR analysis of M2 marker genes *Mrc1* (**G**), *Arg1* (**H**), *Fizz1* (**I**), *Ym1* (**J**) in the tumor tissues. (**K**–**M**) WT and *Atp6v0d2*^{-/-} BMDMs were stimulated with LLC TCM for 24 hours with or without PT2385 (20 mM) and PT2385 was added 18 hours prior to the TCM stimulation. Expression of *Arg1* (**K**), *Fizz1* (**L**), and *Ym1* (**M**) was determined by qRT-PCR. Data were assessed by 1-way ANOVA with Dunnett's test and are presented as mean ± SEM. *$P < 0.05$; **$P < 0.01$; ***$P < 0.001$. Scale bars: 100 μm.

taining 0.5% methylcellulose, and 0.5% Tween 80 according to a previous report (37). Once tumor size reached 100–200 mm³ at day 10, WT and *Atp6v0d2*^{-/-} mice were treated with PBS or PT2385 (5 mg/kg) twice daily by oral gavage for 4 consecutive days. Tumor sizes were measured and recorded daily. On day 14, mice were sacrificed and tumor tissues were collected for experiments.

Cell culture and collection of TCM. Primary BMDMs were generated by culturing mouse BM cells in the presence of 50 ng/ml M-CSF–containing medium for 7 days. BMDMs were seeded in 12-well plates. For the neutralization experiment, BMDMs were stimulated with LLC-derived TCM in the presence of 10 μg/ml different neutralizing antibodies: anti–IL-1β (clone B122; Bio X Cell), anti–IL-6 (clone MP5-20F3; eBioscience), anti–IL-10 (clone JES5-2A5; eBioscience), and anti–TGF-β (clone 19D8; Biolegend). LLC cells and B16-F10 melanoma cells were obtained from ATCC. Cells (1 × 10⁶) were cultured in 10-cm plates with DMEM medium supplemented with 10% heat-inactivated FCS, 100 U/ml penicillin G, and 100 μg/ml streptomycin for 5 days. To collect TCM, cultured media were centrifuged at 14,400 *g* for 5 minutes, followed by filtration with 0.2-μm filters.

Determination of lactate concentration in TCM. The lactate concentration was measured using a Lactate Assay Kit (Bioassay Systems, catalog ECLC-100). The mean values and SEM of the lactate concentration were calculated according to the manufacturer's instructions.

qRT-PCR. Total RNA was extracted from tissues or cell lines with TRIzol reagent (Invitrogen). cDNA was synthesized from 1 μg of RNA using the Reverse Transcription Kit (Toyobo) following the manufacturer's protocol. All qRT-PCR was performed by the SYBR Green method on a Bio-Rad CFX Connect. The quantification of the results was performed by the comparative Ct (2^{-ΔΔCt}) method. The Ct value for each sample was normalized to the value for the *Actin* or *Gapdh* gene. Primer sequences for the *Atp6v0d2*, *Atp6v0a2*, *Atp6v0c*, *Atp6v0d1*, *Atp6v1a*, *Atp6v1c1*, *Atp6v1d*, *Atp6v1e1*, *Atp6v1g1*, *Atp6v13*, *Vegf*, *Glut1*, *Pai1*, *Ccnd1*, *Il1b*, *Il6*, *Hif2a*, *Hif1a*, *Arg1*, *Ym1*, *Fizz1*, *Mrc1*, and *Actb* genes are provided in Supplemental Table 1.

ChIP assay. Mouse BMDM/Raw 264.7 cells were treated with TCM or lactate for 6 hours, followed by cross-linking for 8 minutes with 1% (vol/vol) formaldehyde. Cells were collected and lysed by sonication. Cell lysates were immunoprecipitated with anti-TFEB (ab2636, Abcam). After washing and elution, crosslinks were reversed for 4 hours at 65°C. The eluted DNA was purified and analyzed by qPCR with custom-designed primers (forward, AAACTGGGCAT-

GACCTTG; reverse, GCAGCTCAGAAGGCACA) using a Bio-Rad SYBR Green intercalating fluorophore system. The Ct value for each sample was normalized to the corresponding input value.

Isolation of TAMs. On day 15, mice were sacrificed and tumor tissues were gently minced and excised into small pieces. Afterwards, tumor tissues were disrupted with 1× PBS containing 200 ng/ml collagenase IV (catalog c17104019, Invitrogen), 250 ng/ml hyaluronidase (catalog H1115000, MilliporeSigma), 40 ng/ml DNase I (catalog 10104159001, Roche) at 37°C on a shaker at 100 rpm. Cell suspensions were filtered and red blood cells were lysed. Tumor-infiltrating lymphocytes were separated by gradient centrifugation with 40%/80% Percoll (GE). Collected cells were stained and analyzed by flow cytometry.

Flow cytometry. Single-cell suspensions of tumors were generated following the manufacturer's protocol. After Fc blockade with anti-CD16/CD32 (clone 93), cells were stained with the following antibodies: CD4-FITC (clone RM4-5), CD8-PE (clone 536.7), CD11c-PE (clone N418), F4/80-PerCPcy5.5 (clone BM8), CD206-PE/cy7 (clone C068C2), and CD11b-FITC (clone M1/70) (all from Biolegend). For intracellular staining, cells were stimulated with 50 ng/ml PMA (MilliporeSigma) and 500 ng/ml ionomycin (MilliporeSigma) in the presence of 5 μg/ml GolgiPlug (BD) in complete RPMI 1640 medium for 4 hours at 37°C. Cells were fixed, permeabilized, and stained with the following antibodies: Foxp3-APC (clone FJK-16s; eBioscience), IL-1β–APC (clone NJTEN3; eBioscience), and IFN-γ–BV421 (clone XMG1.2; Biolegend). Samples were collected on a BD FACSVerse flow cytometer, and data were analyzed using FlowJo software (Tree Star).

ELISA quantitation of VEGF. Tumor tissues (0.5 g) were homogenized with 500 μl ice-cold PBS, and then supernatants were collected after centrifugation, and stored at –80°C until further use. VEGF-A in the tumor tissue was measured with an ELISA Kit from Biolegend (DKW12-2734-048) according to the manufacturer's instructions.

Immunofluorescence. BMDMs were seeded at 3 × 10⁴ cells per well in glass slides, and incubated overnight for proper attachment. Then the cells were stimulated with MG132 (20 μM) for 4 hours, and then treated with 1:10,000 PBS-diluted LysoTracker Red DND-99 dye (DMSO solution, Life Technologies) for 15 minutes. After the treatment, cells were washed twice with sterile PBS and fixed with 4% paraformaldehyde, permeabilized with 0.05% Triton X-100, and blocked in 5% BSA. Anti–HIF-2α (NB100-132, Novus) was incubated with the cells overnight at 4°C. Secondary fluorescent antibodies labeled with FITC and Cy3 (from Life Technologies or Jackson Laboratories) were added for 1 hour and DAPI was used for nuclear counterstaining. The human tumor tissues were collected during surgery and fixed in formalin immediately, followed by standard paraffin embedding and immunohistochemistry (22). For human tissue, immunofluorescence staining was performed overnight with antibodies against CD3 (GB13014, Servicebio), CD19 (GB11061, Servicebio), CD68 (ab125212, Abcam), CD31 (GB13063, Servicebio), α-SMA (GB13044, Servicebio), F4/80 (GB11027, Servicebio), and ATP6V0d2 (ab194557, Abcam). Secondary fluorescent antibodies (FITC, Cy3 from Life Technologies or Jackson Laboratories) were added for 1 hour and DAPI was used for nuclear counterstaining. Samples were imaged through an SP5 confocal microscope (Leica) 24 hours after mounting.

Immunoblotting. Immunoblotting was performed according to standard methods. Primary antibodies included the following: phospho-PS6 (4851, Cell Signaling Technology), lamin B1 (13435,
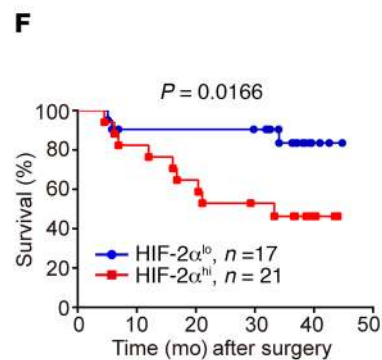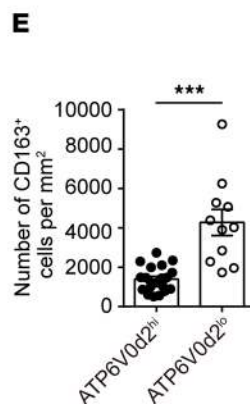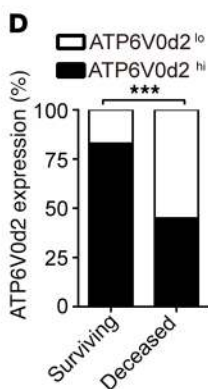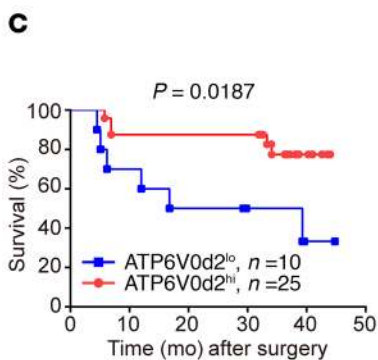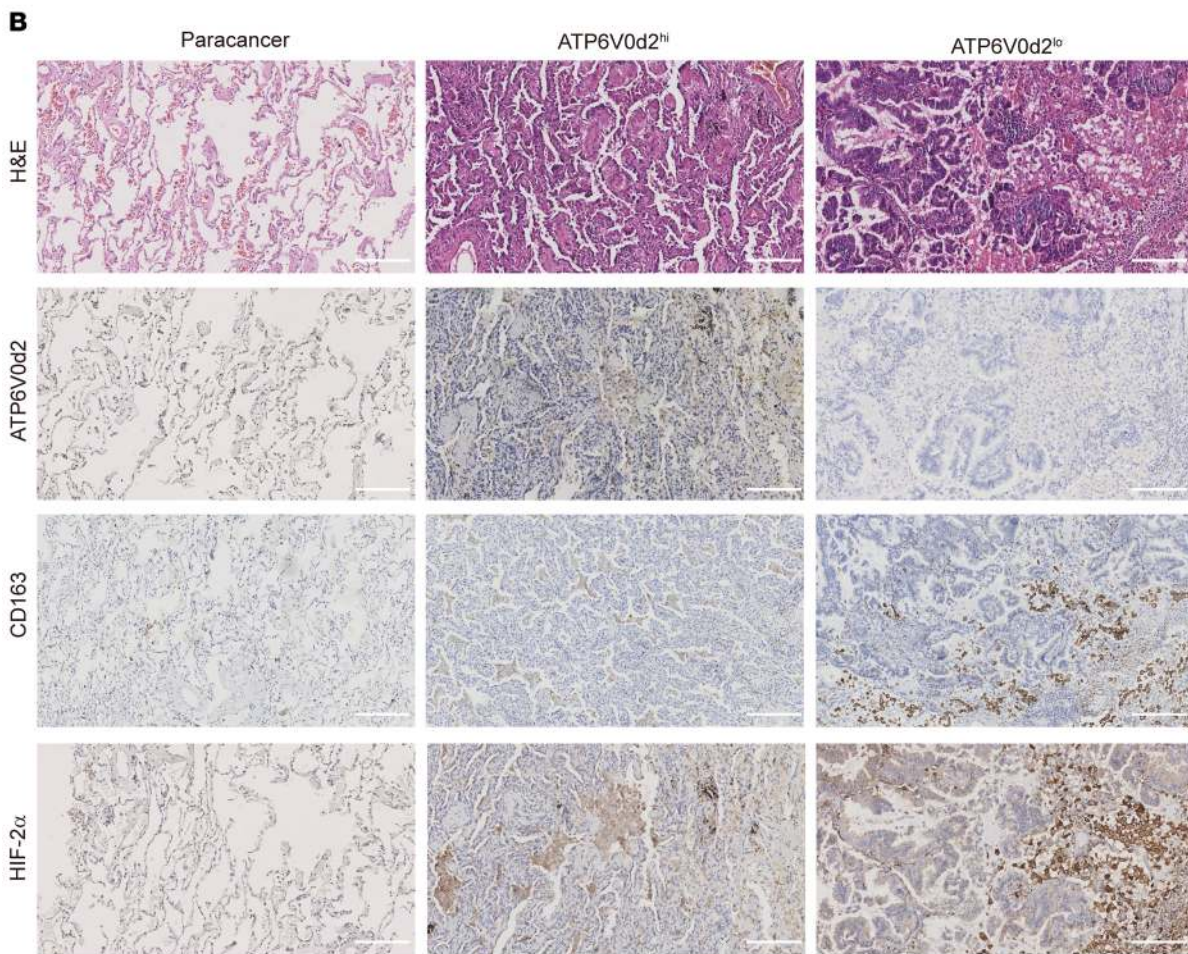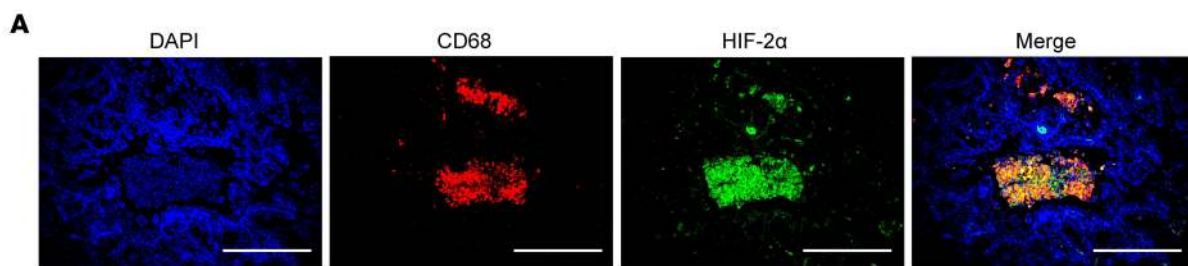
Figure 8. ATP6V0d2 is linked with survival for human lung adenocarcinoma patients. (**A**) Immunofluorescence staining of human primary lung adenocarcinoma tissues with DAPI (blue), anti-CD68 (red), and anti–HIF-2α (green). Scale bars: 200 μm. (**B**) A representative image of H&E staining and immunohistochemical analysis of ATP6V0d2, CD163, and HIF-2α in the lung sections of adjacent nontumorous lungs or tumor tissues isolated from 2 lung adenocarcinoma patients. Scale bars: 50 μm. (**C**) Kaplan-Meier plot of overall survival of patients with lung cancer stratified by high IRS (>3) or low IRS (<3) of ATP6V0d2 expression levels. (**D**) The proportion of ATP6V0d2 expression in surviving and deceased patients was calculated and evaluated by the χ^2 test with GraphPad Prism software. A P value less than 0.05 was considered statistically significant. (**E**) Quantification of numbers of CD163$^+$ TAMs in 5 areas of each patients were determined by IPP image software in 2 groups of lung adenocarcinoma patients with high ATP6V0d2 expression (n = 20, IRS > 3) and low ATP6V0d2 expression (n = 11, IRS < 3). Data are the mean ± SEM. (**F**) Kaplan-Meier plot of overall survival of patients with lung cancer stratified by high IRS (>3) or low IRS (<3) of HIF-2α expression levels. ***P < 0.001 by Student's t test.

Cell Signaling Technology), TFEB (ab2636, Abcam), GAPDH (5174, Cell Signaling Technology), HIF-2α (NB100-122, Novus), HIF-1α (14179S, Cell Signaling Technology), LC3B (12741, Cell Signaling Technology), p62 (PM045, MBL), ATP6V0d2 (SAB2103221, MilliporeSigma), and β-actin (4970S, Cell Signaling Technology). After washing, primary antibodies were followed by appropriate secondary HRP-conjugated antibodies, then developed with ECL reagent (GE Healthcare).

Immunohistochemistry. Paired cancer and adjacent noncancer tissue samples were obtained with informed consent from Tongji Hospital of HUST. The specimens were isolated at the time of surgery, formalin fixed and paraffin embedded, and stained with H&E. Standard immunohistochemistry was performed with antibodies against ATP6V0d2 (ab194557, Abcam), CD163 (ZM-0428, ZSGB-BIO), CD68 (66231-2-Ig, ProteinTech), HIF-2α (NB100-132, Novus Biologicals), then examined by 2 blinded pathologists. The immunoreactive score (IRS) gives a range of 0–8 as a product of multiplication between the positive cell proportion (score 0–4) and staining intensity (score 0–3). To measure the expression of ATP6V0d2, the following IRS assignments were used: 0, negative; 1, mild; 2, moderate; 3, strongly positive. To measure the expression of HIF-2α, the following IRS assignments

were used: 0–1, negative; 2–3, mild; 4–6, moderate, 7–8, strongly positive. The diagnosis of lung cancer or normal lung was confirmed based on histological findings by 2 independent pathologists. The immunohistochemical data were evaluated by 2 blinded pathologists.

Statistics. Data were graphed using GraphPad Prism software. Statistical significance was determined by unpaired 2-tailed Student's t test, 1-way ANOVA followed by Turkey's post hoc test, or 2-way ANOVA. A P value of less than 0.05 was considered significant.

Study approval. All mouse studies were approved and used in accordance with institutional guidelines (Tongji Medical College, HUST). Human specimens used in this study have been approved by the Ethics Committee of Tongji Hospital, Huazhong University of Science and Technology, and signed informed consent was obtained from all patients' families (TJ-IRB-20180516, Tongji Hospital, HUST, Wuhan).

Author contributions

NL, JL, AL, and XPY conceptualized the study. NL, JL, DK, SX, YD, YX, ZW, XX, FC, SL, H. Liu, and JW carried out the investigations. BY, KJ, FG, ZT, XC, ZL, GW, and XPY conducted formal analyses of the data. H. Li and GW provided resources. FG and XPY acquired funding and supervised the study. NL, JL, AL, and XPY prepared the data and figures and wrote the manuscript.

Address correspondence to: Guoping Wang, Institute of Pathology, Tongji Hospital, HUST, 1095 Jiefang Road, Wuhan, 430030, China. Phone: 86.27.83662856; Email: wanggp@hust.edu.cn. Or to: Xiang-Ping Yang, Department of Immunology, Tongji Medical College, Huazhong University of Science and Technology, 13 Hangkong Road, Wuhan, 430030, China. Phone: 86.27.83692600; Email: yangxp@hust.edu.cn.

1. Murray PJ, et al. Macrophage activation and polarization: nomenclature and experimental guidelines. *Immunity*. 2014;41(1):14–20.
2. Epelman S, Lavine KJ, Randolph GJ. Origin and functions of tissue macrophages. *Immunity*. 2014;41(1):21–35.
3. Ruffell B, Coussens LM. Macrophages and therapeutic resistance in cancer. *Cancer Cell*. 2015;27(4):462–472.
4. Quail DF, Joyce JA. Microenvironmental regulation of tumor progression and metastasis. *Nat Med*. 2013;19(11):1423–1437.
5. Qian BZ, Pollard JW. Macrophage diversity enhances tumor progression and metastasis. *Cell*. 2010;141(1):39–51.
6. Sica A, Mantovani A. Macrophage plasticity and polarization: in vivo veritas. *J Clin Invest*. 2012;122(3):787–795.
7. Gordon S, Martinez FO. Alternative activation of macrophages: mechanism and functions. *Immu-*

nity. 2010;32(5):593–604.
8. Stockmann C, et al. Deletion of vascular endothelial growth factor in myeloid cells accelerates tumorigenesis. *Nature*. 2008;456(7223):814–818.
9. Murdoch C, Muthana M, Coffelt SB, Lewis CE. The role of myeloid cells in the promotion of tumour angiogenesis. *Nat Rev Cancer*. 2008;8(8):618–631.
10. Pugh CW, Ratcliffe PJ. Regulation of angiogenesis by hypoxia: role of the HIF system. *Nat Med*. 2003;9(6):677–684.
11. Brahimi-Horn MC, Pouysségur J. HIF at a glance. *J Cell Sci*. 2009;122(Pt 8):1055–1057.
12. Lee DC, et al. A lactate-induced response to hypoxia. *Cell*. 2015;161(3):595–609.
13. Colegio OR, et al. Functional polarization of tumour-associated macrophages by tumour-derived lactic acid. *Nature*. 2014;513(7519):559–563.
14. Levine B, Kroemer G. Autophagy in the patho-

genesis of disease. *Cell*. 2008;132(1):27–42.
15. Cotter K, Stransky L, McGuire C, Forgac M. Recent insights into the structure, regulation, and function of the V-ATPases. *Trends Biochem Sci*. 2015;40(10):611–622.
16. McGuire C, Cotter K, Stransky L, Forgac M. Regulation of V-ATPase assembly and function of V-ATPases in tumor cell invasiveness. *Biochim Biophys Acta*. 2016;1857(8):1213–1218.
17. McGuire C, Stransky L, Cotter K, Forgac M. Regulation of V-ATPase activity. *Front Biosci (Landmark Ed)*. 2017;22:609–622.
18. Settembre C, et al. A lysosome-to-nucleus signalling mechanism senses and regulates the lysosome via mTOR and TFEB. *EMBO J*. 2012;31(5):1095–1108.
19. Settembre C, et al. TFEB links autophagy to lysosomal biogenesis. *Science*. 2011;332(6036):1429–1433.
20. Holmquist-Mengelbier L, et al. Recruitment of

HIF-1alpha and HIF-2alpha to common target genes is differentially regulated in neuroblastoma: HIF-2alpha promotes an aggressive phenotype. *Cancer Cell*. 2006;10(5):413–423.

21. Carroll VA, Ashcroft M. Role of hypoxia-inducible factor (HIF)-1alpha versus HIF-2alpha in the regulation of HIF target genes in response to hypoxia, insulin-like growth factor-I, or loss of von Hippel-Lindau function: implications for targeting the HIF pathway. *Cancer Res*. 2006;66(12):6264–6270.

22. Talks KL, et al. The expression and distribution of the hypoxia-inducible factors HIF-1alpha and HIF-2alpha in normal human tissues, cancers, and tumor-associated macrophages. *Am J Pathol*. 2000;157(2):411–421.

23. Amit I, Winter DR, Jung S. The role of the local environment and epigenetics in shaping macrophage identity and their effect on tissue homeostasis. *Nat Immunol*. 2016;17(1):18–25.

24. Ruan GX, Kazlauskas A. Lactate engages receptor tyrosine kinases Axl, Tie2, and vascular endothelial growth factor receptor 2 to activate phosphoinositide 3-kinase/Akt and promote angiogenesis. *J Biol Chem*. 2013;288(29):21161–21172.

25. Allen E, et al. Metabolic symbiosis enables adaptive resistance to anti-angiogenic therapy that is dependent on mTOR signaling. *Cell Rep*. 2016;15(6):1144–1160.

26. Peri F, Nüsslein-Volhard C. Live imaging of neuronal degradation by microglia reveals a role for V0-ATPase A1 in phagosomal fusion in vivo. *Cell*. 2008;133(5):916–927.

27. Leek RD, et al. Relation of hypoxia-inducible factor-2 alpha (HIF-2 alpha) expression in tumor-infiltrative macrophages to tumor angiogenesis and the oxidative thymidine phosphorylase pathway in Human breast cancer. *Cancer Res*. 2002;62(5):1326–1329.

28. Imtiyaz HZ, et al. Hypoxia-inducible factor 2alpha regulates macrophage function in mouse models of acute and tumor inflammation. *J Clin Invest*. 2010;120(8):2699–2714.

29. Greer SN, Metcalf JL, Wang Y, Ohh M. The updated biology of hypoxia-inducible factor. *EMBO J*. 2012;31(11):2448–2460.

30. Harris AL. Hypoxia--a key regulatory factor in tumour growth. *Nat Rev Cancer*. 2002;2(1):38–47.

31. Hubbi ME, Hu H, Kshitiz, Ahmed I, Levchenko A, Semenza GL. Chaperone-mediated autophagy targets hypoxia-inducible factor-1alpha (HIF-1alpha) for lysosomal degradation. *J Biol Chem*. 2013;288(15):10703–10714.

32. Hubbi ME, et al. Cyclin-dependent kinases regulate lysosomal degradation of hypoxia-inducible factor 1alpha to promote cell-cycle progression. *Proc Natl Acad Sci U S A*. 2014;111(32):E3325–E3334.

33. Liu XD, et al. Autophagy mediates HIF2α degradation and suppresses renal tumorigenesis. *Oncogene*. 2015;34(19):2450–2460.

34. Munksgaard Persson M, et al. HIF-2α expression is suppressed in SCLC cells, which survive in moderate and severe hypoxia when HIF-1α is repressed. *Am J Pathol*. 2012;180(2):494–504.

35. Ohtaki Y, et al. Stromal macrophage expressing CD204 is associated with tumor aggressiveness in lung adenocarcinoma. *J Thorac Oncol*. 2010;5(10):1507–1515.

36. Rolny C, et al. HRG inhibits tumor growth and metastasis by inducing macrophage polarization and vessel normalization through downregulation of PlGF. *Cancer Cell*. 2011;19(1):31–44.

37. Wallace EM, et al. A small-molecule antagonist of HIF2α is efficacious in preclinical models of renal cell carcinoma. *Cancer Res*. 2016;76(18):5491–5500.